Core–shell Au/Ag nanoparticles embedded in silicate sol–gel network for sensor application towards hydrogen peroxide[†]

SHANMUGAM MANIVANNAN and RAMASAMY RAMARAJ*

Centre for Photoelectrochemistry, School of chemistry, Madurai Kamaraj University, Madurai 625 021
e-mail: ramarajr@yahoo.com

Abstract. The electrocatalytic activity of core–shell $Au_{100-x}Ag_x$ ($x = 15$, 27, 46, and 60) bimetallic nanoparticles embedded in methyl functionalized silicate MTMOS network towards the reduction of hydrogen peroxide was investigated by using cyclic voltammetry and chronoamperometric techniques. Core–shell Au/Ag bimetallic nanoparticles were characterized by absorption spectra and HRTEM. The MTMOS silicate sol–gel embedded $Au_{73}Ag_{27}$ core–shell nanoparticles modified electrode showed better synergistic electrocatalytic effect towards the reduction of hydrogen peroxide when compared to monometal MTMOS-Au_{nps} and MTMOS-Ag_{nps} modified electrodes. These modified electrodes were studied without immobilizing any enzyme in the MTMOS sol–gel matrix. The present study highlights the influence of molar composition of Ag nanoparticles in the Au/Ag bimetallic composition towards the electrocatalytic reduction and sensing of hydrogen peroxide in comparison to monometal Au and Ag nanoparticles.

Keywords. Core–shell Au/Ag nanoparticles; modified electrode; electrocatalysis; hydrogen peroxide; sensor.

1. Introduction

Bimetallic nanoparticles are receiving much attention due to their specific electronic, optical and catalytic properties that are different from those of the corresponding monometal nanoparticles.[1–3] It is well-known that the addition of a second metallic component enhances the activity, selectivity and stability of a pure monometal catalyst.[3] The properties of bimetal nanoparticles can vary dramatically not only with size, as happens in pure nanoclusters, but also with chemical composition.[3–6] The catalytic and electronic properties of bimetallic nanomaterials can be tailored by changing the composition and structure, because of the formation of unique surface upon the addition of a second metal to a conventional metal catalyst. It has been reported in many cases that bimetallic systems display a core–shell structure, where a thin shell of second metal surrounds a core of first metal. The second metal over layer is usually strained, and thus can present prominent catalytic properties, which gives raise to the so called synergistic catalytic effect.[4–11] Nanocomposites of core–shell structures are studied because of their

bifunctional activity and also there has been some deviation in the activity when the core and shell are interchanged with each other.[12]

The bimetallic nanoparticles modified electrode sensors are attracting attention in recent years since the electrochemical sensors are an extremely active area of nanoscience research.[13] Electrodes modified with thin films of silicate sol–gel network exhibit physical rigidity, biodegradation, electrochemical, photochemical, thermal stabilities and optical transparency.[14–17] The nanoparticles embedded in silicate sol–gel network tends to exhibit extremely narrow size distribution if the metal nanoparticle concentrations are kept low. Such nanoparticles dispersed silicate sol–gel networks are very much useful in heterogeneous catalysis and chemical sensors.[18]

The hydrogen peroxide sensors are of practical importance in chemical, biological, clinical, environmental and fuel cell applications.[19–21,22] Gao *et al*[23] reported the gold nanoparticles-Hb (Hemoglobin) system for hydrogen peroxide sensing. Wu *et al*[24] reported the silver-DNA hybrid nanoparticles for sensing hydrogen peroxide and Yang *et al*[25] reported myoglobin and gold nanoparticles incorporated Nafion modified electrodes for sensing hydrogen peroxide. The hydrogen peroxide biosensor based on horseradish peroxidase immobilized on

---

colloidal gold was found to be electrocatalytically active in the reduction of hydrogen peroxide.[26] Considerable attention was given in the fabrication of hydrogen peroxide sensor based on metal nanoparticles modified electrodes.[27–30]

The present work deals with the preparation and characterization of Au/Ag core–shell nanoparticles in methyl functionalized silicate (MTMOS) sol–gel matrix with four different Au/Ag compositions. These nanocolloids in MTMOS silicate sol–gel matrix were used to modify the glassy carbon electrode. Cyclic voltammetric and chronoamperometric techniques were used to evaluate the electrocatalytic activity of the core–shell bimetal nanoparticles modified electrodes towards hydrogen peroxide reduction. The influence of molar composition of Ag in the Au/Ag bimetallic composition on the electrocatalytic reduction of hydrogen peroxide was studied and the results were compared with monometal Au and Ag nanoparticles modified electrodes.

2. Experimental

2.1 *Chemicals and methods*

$HAuCl_4·6H_2O$ and $AgNO_3$ were obtained from SRL. Methyltrimethoxysilane (MTMOS), sodium citrate tribasic dihydrate ($Na_3C_6H_5O_7·2H_2O$) and H_2O_2 were obtained from Merck. All glassware were thoroughly cleaned with aqua regia ($3:1$ HNO_3/HCl (v/v)) and rinsed extensively with doubly distilled water before use. All aqueous solutions were prepared using doubly distilled water. Spectroscopic studies were performed using Agilent Technologies 8453 spectrophotometer. The size of the metal nanoparticles was characterized by high resolution transmission electron microscopy (HRTEM) using FEI TECNAI 30 G^2 S-TWIN instrument and carbon coated Cu Grid.

2.2 *Preparation of core–shell Au/Ag bimetallic nanoparticles*

The $Au_{100-x}Ag_x$ core–shell nanoparticles stabilized by citrate were prepared by following reported procedure.[12] In a typical experiment, aliquots of 1 mM $AgNO_3$ (250, 500, 1000 and 2000 μL) were added drop-by-drop to 5 mL of a preformed citrate-reduced Au nanoparticles[31] with continuous stirring. Then the corresponding volume of the citrate solution was added to $AgNO_3$ solution to induce the reduction of

Ag^+ and its deposition on Au nanoparticles. The mixture was kept boiling for 1 h. The percentage compositions of the resulting core–shell bimetallic colloids were $Au_{85}Ag_{15}$, $Au_{73}Ag_{27}$, $Au_{54}Ag_{46}$ and $Au_{40}Ag_{60}$. Monometal silver nanoparticles were prepared by citrate reduction method.[32]

2.3 *Dispersion of core–shell Au/Ag nanoparticles in MTMOS silicate sol–gel matrix*

The homogeneous MTMOS sol–gel matrix was prepared[33] by using a mixture of EtOH/MTMOS/0·1 M HCl in the ratio $7·50:3·75:1·00$ (v/v). A known amount of MTMOS sol–gel and Au/Ag core–shell bimetal nanoparticles solutions were mixed (50 : 1, 75 : 1, and 100 : 1 mole ratios of Si to Au) under stirring for 3 min. An immediate colour change was observed for the mixed solution, indicating the dispersion of metal nanoparticles in the MTMOS sol–gel matrix.

2.4 *Preparation of modified electrodes*

The GC electrode (dia = 3 mm, CH Instruments, USA) was twice polished using alumina powder (0·05 micron) followed by sonication in doubly distilled water for 3 min. The cleaned GC electrode was dried for 5 min at room temperature. A known volume of the mixture containing MTMOS silicate sol–gel and Ag_{nps} or Au_{nps} or $Au_{100-x}Ag_x$ core–shell nanoparticles was casted on the surface of the GC electrode and allowed to dry at room temperature for 1 hour (represented as GC/MTMOS-Au_{nps}, GC/MTMOS-Ag_{nps}, and GC/MTMOS $Au_{100-x}Ag_x$). The dried electrode was then dipped in water for 10 min and used for the electrochemical experiments. Film thickness of modified electrode was calculated as 1 μm.[33,34]

2.5 *Electrochemistry*

Cyclic voltammograms were carried out using an EG&G Princeton Applied Research 283 Potentiostat/Galvanostat controlled by Echem software. Electrochemical experiments were performed using a single compartment three-electrode cell. The reference electrodes were a saturated calomel electrode (SCE) for cyclic voltammetry experiments and Ag/AgCl electrode for chronoamperometry experiments. The modified glassy carbon (GC) electrode

was used as working electrode and Pt wire was used as counter electrode.

3. Results and discussion

3.1 *Spectroscopic studies of Au, Ag and Au$_{100-x}$Ag$_x$ nanoparticles*

The absorption spectra of Ag and Au nanoparticles showed bands at 407 and 519 nm, respectively (figure 1a) due to their corresponding plasmon excitation resonance.[31,32,35] Figure 1b shows the absorption spectra obtained for Au/Ag core–shell nanoparticles (Au$_{100-x}$Ag$_x$). In the Au/Ag core–shell nanoparticles, the increase of Ag composition leads to a blue shift in the absorption band of Au/Ag bimetal nanoparticles with respect to Au$_{nps}$. Distinguished absorption bands for both Ag and Au in the Au/Ag bimetal

Figure 1. Surface plasmon absorption spectra obtained for gold, silver (**a**) and core–shell Au/Ag, (**b**) nanoparticles.

nanoparticles were observed at increased Ag composition (Figure 1b) suggesting the presence of both Ag and Au in the nanoparticles. The percentage composition of Au$_{100-x}$Ag$_x$ core–shell nanoparticles was tuned by simply varying the AgNO$_3$ concentration. It confirms the formation of Au/Ag core–shell nanostructure over the alloy structure, because alloy structure gives only one absorption maximum depending on the metallic composition.[36]

3.2 *HRTEM characterization of Au, Ag and Au$_{100-x}$Ag$_x$ nanoparticles*

Figure 2 depicts the representative HRTEM images of Au, Ag, Au$_{73}$Ag$_{27}$ and Au$_{40}$Ag$_{60}$ nanoparticles. The average particle size of Au$_{nps}$ was estimated as 16 nm from Figure 2a and the average particle size of Ag$_{nps}$ was estimated as 20 to 25 nm from figure 2b. The size and shape (figure 2c) of the Au$_{73}$Ag$_{27}$ nanoparticles are somewhat interesting, i.e. the size matches with the Au nanoparticles and the shape resembles with the morphology of Ag nanoparticles (figure 2b) which suggests that the thickness of the silver shell is very thin. The Ag shell thickness was estimated as ≈ 3 nm for Au$_{40}$Ag$_{60}$ from the HRTEM image.

3.3 *Characterization of Au, Ag and Au$_{100-x}$Ag$_x$ nanoparticles embedded in MTMOS sol–gel matrix*

The absorption spectrum of core–shell Au$_{73}$Ag$_{27}$ bimetal nanoparticles embedded in MTMOS sol–gel matrix (Si : Au = 100 : 1) (figure 3C) showed a small red shift, where as the Au nanoparticles mixed with MTMOS network (Si : Au = 100 : 1) showed (figure 3A) a new band at 610 nm in addition to the 519 nm band. The new band observed for Au$_{nps}$ in MTMOS sol–gel matrix suggests that the Au nanoparticles interact with the MTMOS silicate matrix leading to some agglomerization of Au$_{nps}$. The Ag nanoparticles embedded in MTMOS network (figure 3B) showed a small red shift and new broad band at a higher wavelength region. This observation reveals the interaction between the Ag nanoparticles and MTMOS silicate network leading to some agglomerization.

3.4 *Electrochemical impedance spectroscopy (EIS) studies*

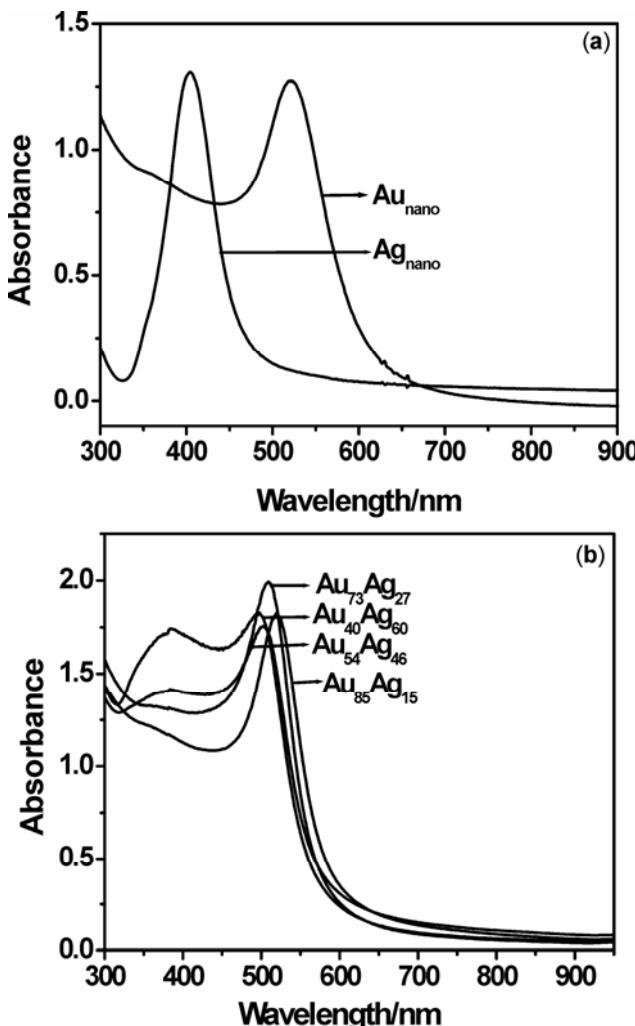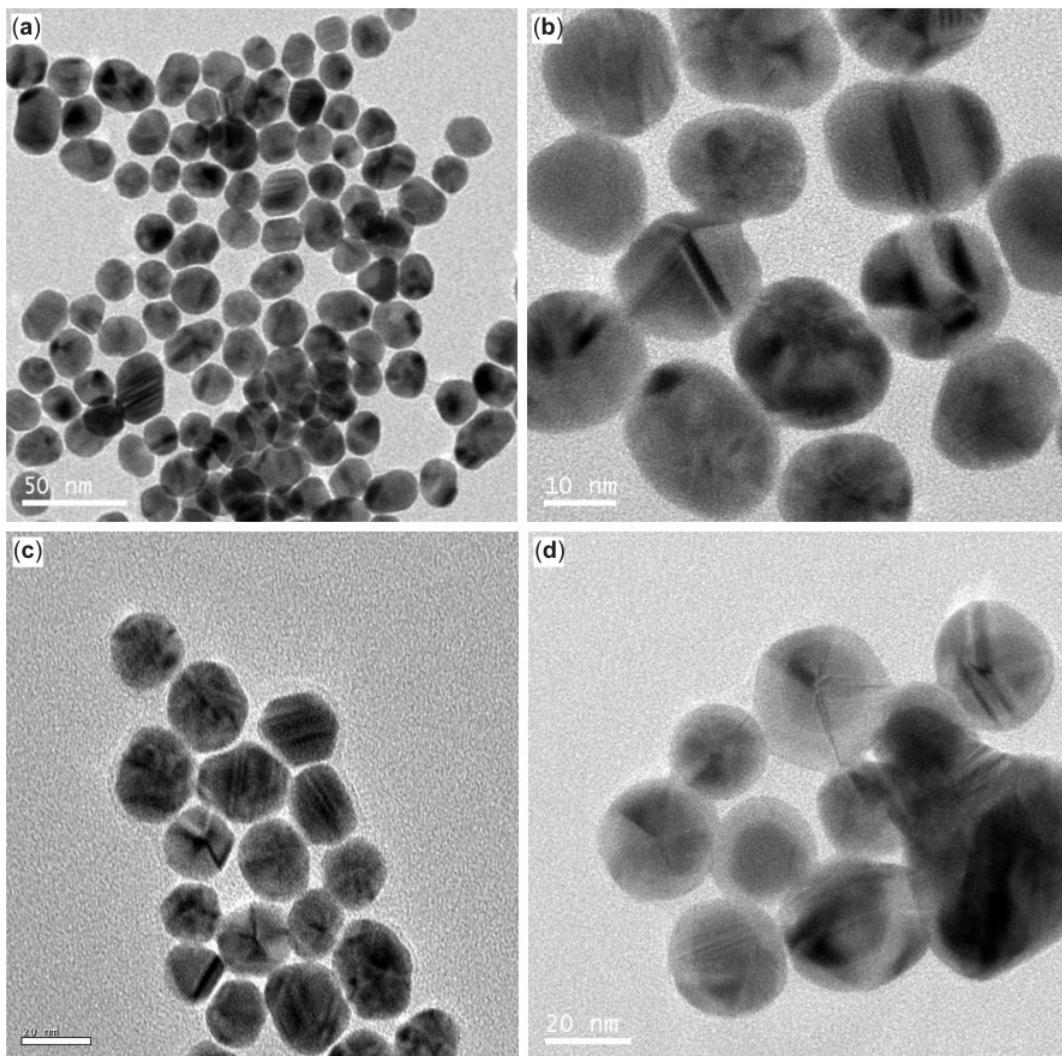EIS studies were carried out to understand the interfacial properties of Au/Ag embedded in MTMOS

Figure 2. HRTEM images of Au (**a**), Ag (**b**), $Au_{73}Ag_{27}$ (**c**) and $Au_{40}Ag_{60}$ (**d**) nanoparticles.

sol–gel modified electrodes. For impedance measurements, a small sinusoidal AC voltage probe is applied, and the current response is determined. In-phase current response determines the real (resistive) component of the impedance, while the out of phase current response determines the imaginary (capacitive) component. The AC voltage should be small enough so that the system response is linear, allowing simple equivalent circuit analysis. The $[Fe(CN)_6]^{3-/4-}$ couple was used as redox probe to study the impedance properties of GC/MTMOS, GC/MTMOS-Au_{nps}, GC/MTMOS-Ag_{nps} and GC/MTMOS-$Au_{100-x}Ag_x$ modified electrodes. The Nyquist diagram of the complex impedance represents the imaginary versus the real part of the impedance. The Nyquist plots show semicircle at higher frequencies corresponding to the electron

transfer limited process and linear portion at lower frequencies corresponding to the diffusion-limited process.[34] Figure 4A shows the response observed at GC/MTMOS, GC/MTMOS-Ag_{nps}, GC/MTMOS-Au_{nps} and GC/MTMOS-$Au_{73}Ag_{27}$ modified electrodes. The EIS was also recorded for bare GC and polycrystalline electrodes (figure not shown). The EIS observations match well with literature for bare GC and polycrystalline Au electrodes.[37,38] In our previous report,[34] we have observed a large increase in charge transfer resistance (R_{ct}) for GC/MTMOS modified electrode due to the silicate matrix film on the GC electrode and the MTMOS film show high hindrance to the electron transfer kinetics. In the present study, the incorporation of Au/Ag core–shell bimetallic nanoparticles into the MTMOS sol–gel matrix lead to a large decrease in the R_{ct} when com-

pared to GC/MTMOS-Ag$_{nps}$, GC/MTMOS-Au$_{nps}$ modified electrodes (figure 4A).
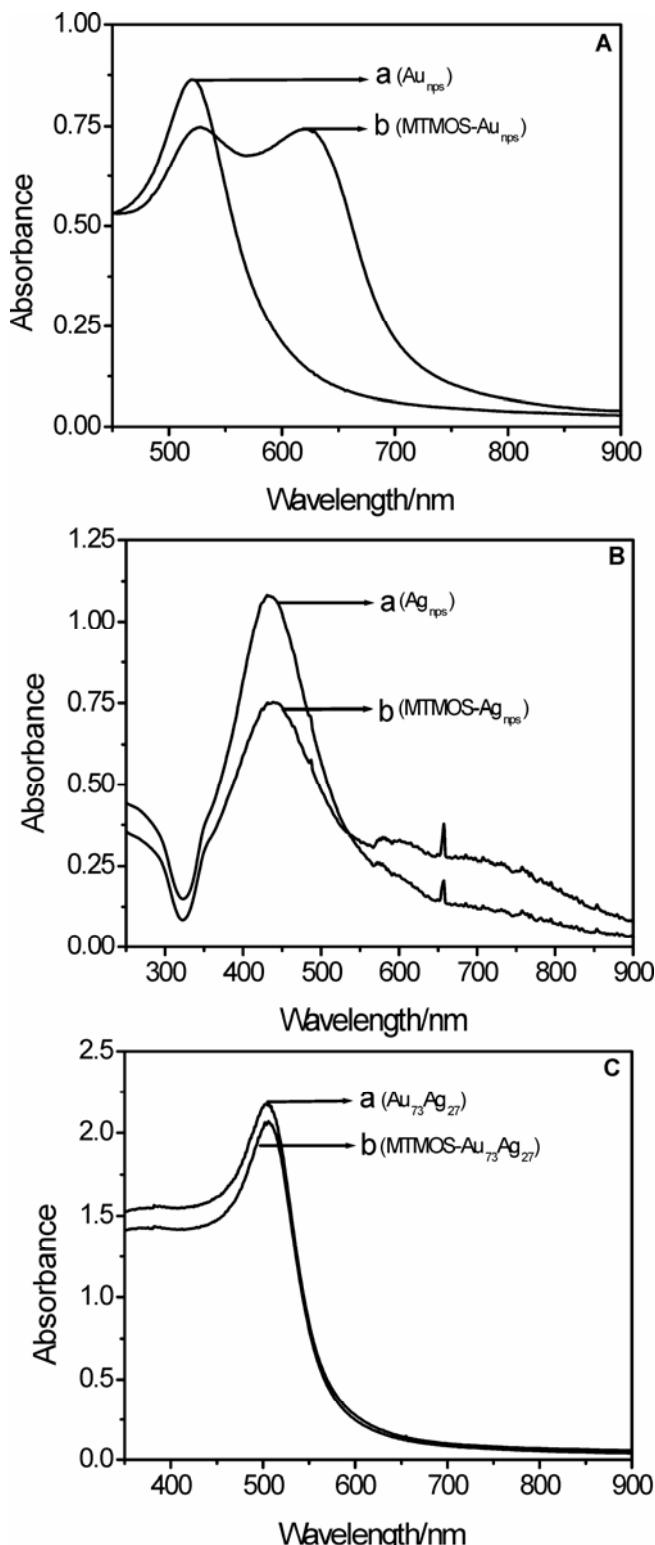
Out of all Au/Ag core–shell nanoparticles, a large decrease in R_{ct} was observed for the Au$_{73}$Ag$_{27}$ core–shell composition (figure 4B). This means that the GC/MTMOSAu$_{73}$Ag$_{27}$ modified electrode shows better conducting effect and facilitates the electron transfer process at the electrode interface when compared to Au$_{nps}$, Ag$_{nps}$ and remaining Au/Ag core–shell nanoparticles modified electrodes. These observations support the synergistic effect exerted by the MTMOS-Au$_{73}$Ag$_{27}$ nanoparticles at the modified electrodes.
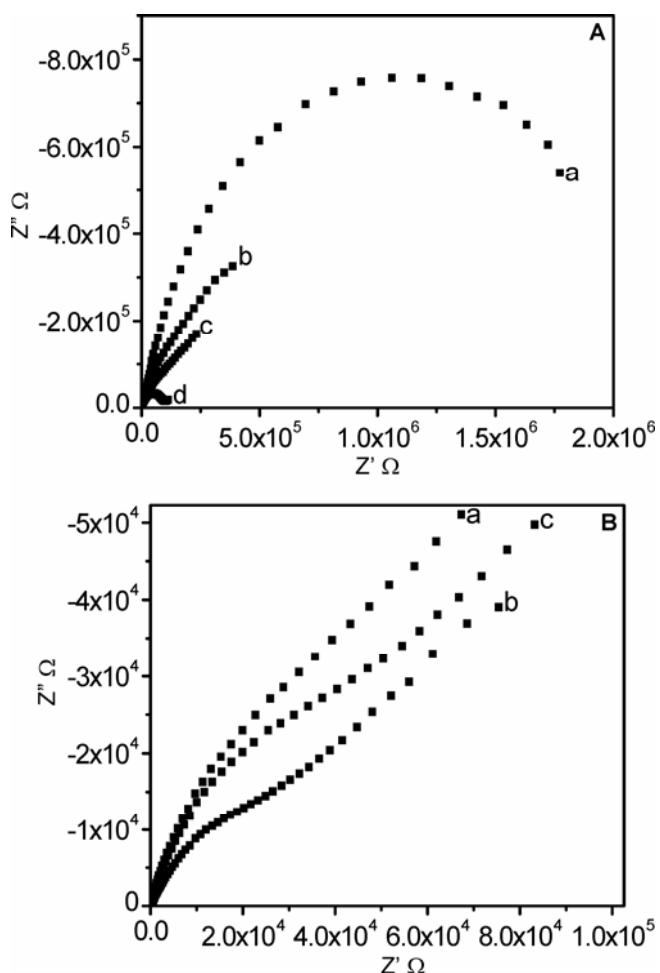

Figure 4A. Electrochemical impedance spectroscopic (EIS) responses observed at GC/MTMOS (a) GC/MTMOS-Ag$_{nps}$, (b) GC/MTMOS-Au$_{nps}$, (c) and GC/MTMOSAu$_{40}$Ag$_{60}$, (d) electrodes. Redox analyte was 1 mM of K$_3$Fe(CN)$_6$ in 0·1 M PBS and 0·1 M KCl. The electrode potential was 0·25 V and the frequency range was 1 Hz to 100 kHz. **B.** Electrochemical impedance spectroscopic (EIS) responses observed at GC/MTMOS-Au$_{85}$Ag$_{15}$, (a) GC/MTMOS-Au$_{73}$Ag$_{27}$, (b) and GC/MTMOS-Au$_{54}$Ag$_{46}$ (c) electrodes. Redox analyte was 1 mM of K$_3$Fe(CN)$_6$ in 0·1 M PBS and 0·1 M KCl. The electrode potential was 0·25 V and the frequency range was 1 Hz to 100 kHz.

Figure 3. Surface plasmon absorption spectra of gold (**A**) silver, (**B**) and Au$_{73}$Ag$_{27}$ core-shell, (**C**) nanoparticles embedded in MTMOS sol–gel matrix.

3.5 Electrochemical characterization of Au$_{nps}$, Ag$_{nps}$ and Au$_{100-x}$Ag$_x$ nanoparticles embedded in MTMOS sol–gel matrix

In order to understand the electrochemical characteristics of Ag$_{nps}$, Au$_{nps}$ and Au$_{100-x}$Ag$_x$ nanoparticles in MTMOS matrix, the cyclicvoltammograms were recorded for GC/MTMOS-Ag$_{nps}$, GC/MTMOS-Au$_{nps}$ and GC/MTMOS-Au$_{100-x}$Ag$_x$ modified electrodes in 0·1 M H$_2$SO$_4$. Figure 5A shows the characteristic cyclic voltammograms of GC/MTMOS-Ag$_{nps}$ and GC/MTMOS-Au$_{nps}$ modified electrodes in 0·1 M H$_2$SO$_4$ at 50 mV s^{-1}. The characteristic oxidation peaks due to monometal Au and Ag nanoparticles
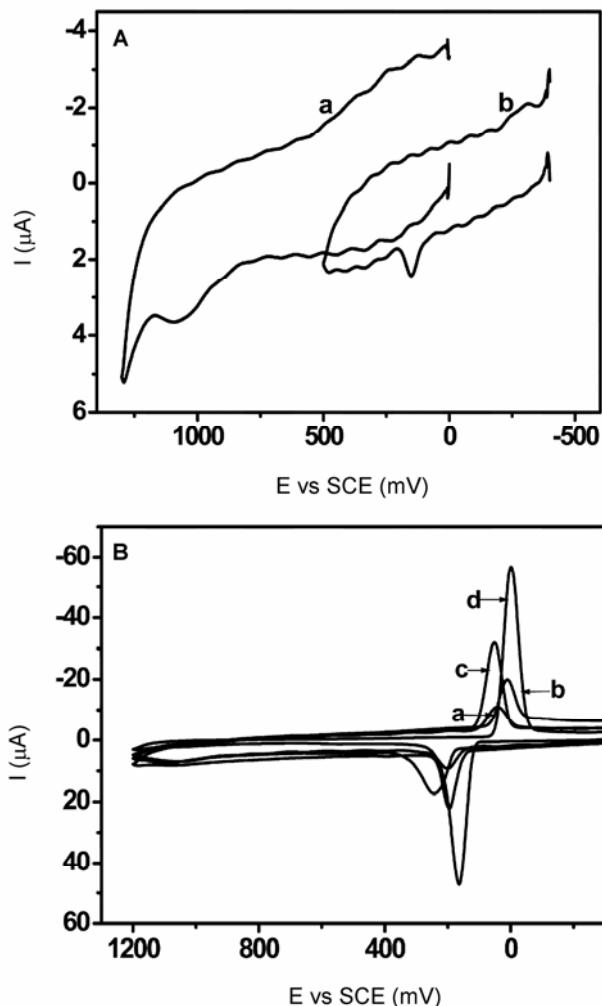

Figure 5A. Cyclic voltammograms recorded for GC/MTMOS-Au$_{nps}$ (a) and GC/MTMOS-Ag$_{nps}$, (b) electrodes in 0·1 M of H2SO4 at a scan rate of 50 mVs^{-1}. **B**, Cyclic voltammograms recorded for GC/MTMOS-Au$_{85}$Ag$_{15}$ (a), GC/MTMOS-Au$_{73}$Ag$_{27}$ (b), GC/MTMOS-Au$_{54}$Ag$_{46}$ (c) and GC/MTMOS-Au$_{40}$Ag$_{60}$ (d) electrodes in 0·1 M of H$_2$SO$_4$ at a scan rate 50 mV s^{-1}.

were clearly observed at 1·1 V and 0·15 V respectively (figure 5A).

In the case of GC/MTMOS-Au$_{100-x}$Ag$_x$ modified electrodes (figure 5B) a large increase in the anodic and cathodic peak currents due to Ag shell in the Au/Ag bimetal core–shell nanoparticles was observed due to the promotional effect of the Au core,[39] and a slight shift in the oxidation potential was also observed depending on the silver composition in the Au/Ag bimetal core–shell nanoparticles.

3.6 Electrocatalytic reduction of H$_2$O$_2$ at GC/MTMOS-Ag$_{nps}$, GC/MTMOS-Au$_{nps}$ and GC/MTMOS-Au$_{100-x}$Ag$_x$ modified electrodes

The electrocatalytic reduction of H$_2$O$_2$ was investigated at the GC/MTMOSAg$_{nps}$, GC/MTMOS-Au$_{nps}$ and GC/MTMOS-Au$_{100-x}$Ag$_x$ modified electrodes at pH 7·2 (PBS). Figure 7A shows the catalytic reduction of H$_2$O$_2$ at bare GC, GC/MTMOS and GC/MTMOS-Au$_{73}$Ag$_{27}$ modified electrodes. Figure 7B shows the comparison of GC/MTMOS-Ag$_{nps}$, GC/MTMOS-Au$_{nps}$ and GC/MTMOS-Au$_{73}$Ag$_{27}$ modified electrodes towards the catalytic reduction of H$_2$O$_2$ in 0·1 M PBS (pH 7·2) at scan rate of 50 mV s^{-1}. No observable H$_2$O$_2$ reduction current was noticed at the bare GC and GC/MTMOS electrodes at the potential window of $-0·1$ to $-0·8$ V (figure 7A). When Au$_{nps}$ or Ag$_{nps}$ was introduced in the MTMOS matrix, an observable cathodic current was noticed at more negative potentials (figure 7B). Figure 7B shows the onset of catalytic reduction of H$_2$O$_2$ from around $-0·5$ V at the GC/MTMOS-Ag$_{nps}$, GC/MTMOS-Au$_{nps}$ modified electrodes. When Au/Ag core–shell nanoparticles were introduced at the
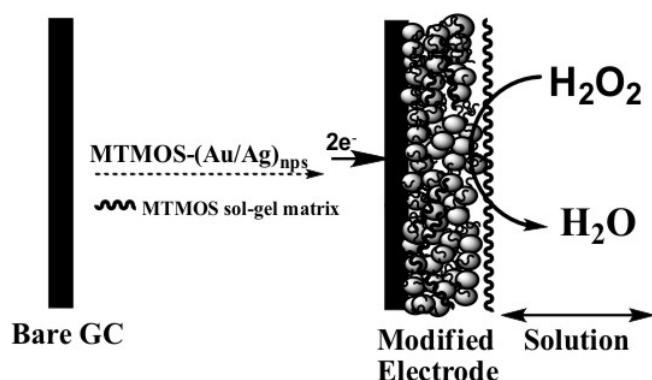

Figure 6. Schematic representation of electrocatalytic reduction of H$_2$O$_2$ at the Au/Ag bimetallic core–shell nanoparticles modified electrode.
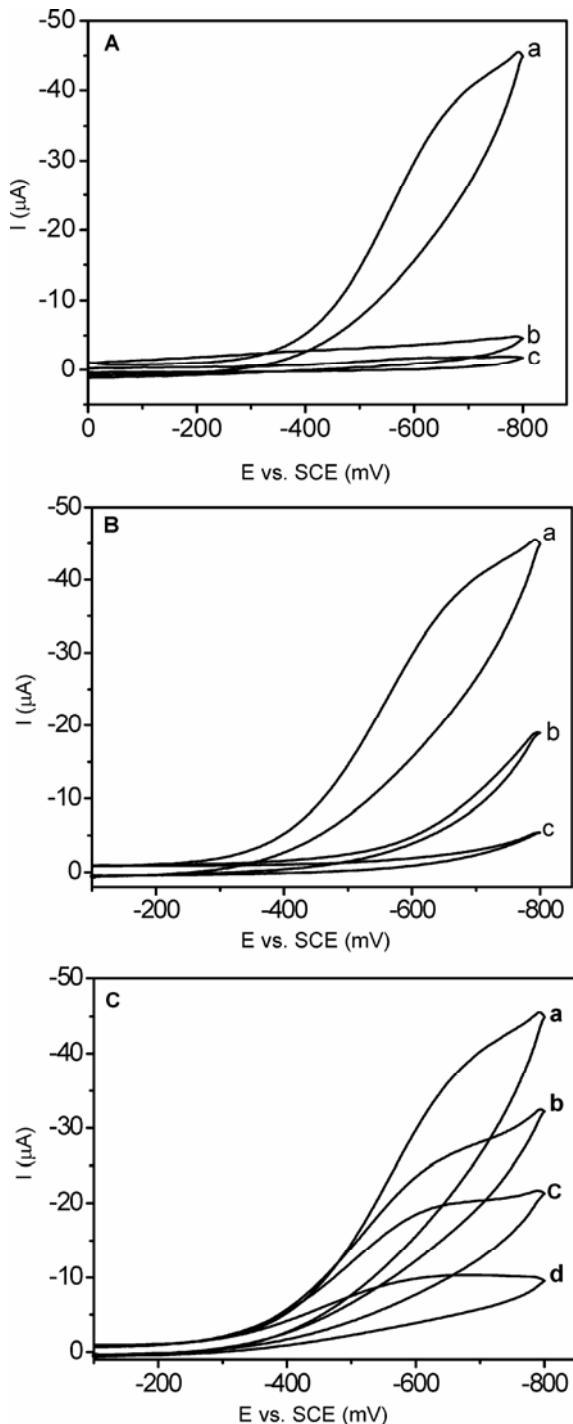
Figure 7A. Cyclic voltammograms recorded for 1 mM of H_2O_2 at GC/MTMOSAu$_{73}$Ag$_{27}$ (a), GC/MTMOS (b) and bare GC (c) electrodes in 0·1 M PBS (pH = 7·2) at a scan rate of 50 mV s^{-1}. **B**, Cyclic voltammograms recorded for 1 mM of H_2O_2 at GC/MTMOSAu$_{73}$Ag$_{27}$ (a), GC/MTMOS-Au$_{nps}$ (b) and GC/MTMOS-Ag$_{nps}$ (c) modified electrodes in 0·1 M PBS (pH = 7·2) at a scan rate of 50 mV s^{-1}. **C**, Cyclic voltammograms recorded for 1 mM of H_2O_2 at GC/MTMOS-Au$_{73}$Ag$_{27}$ (a), GC/MTMOS-Au$_{54}$Ag$_{46}$ (b), GC/MTMOS-Au$_{40}$Ag$_{60}$ (c) and GC/MTMOS-Au$_{85}$Ag$_{15}$ (d) modified electrodes in 0·1 M PBS (pH = 7·2) at a scan rate of 50 mV s^{-1}.

MTMOS sol–gel matrix, the modified electrode showed a large catalytic current with an onset potential of –0·15 V when compared to monometal nanoparticles modified electrodes. The catalytic reduction potential was shifted to more positive potential at the Au/Ag bimetal core–shell nanoparticles modified electrodes. Figure 7C displays the comparison of GC/MTMOSAu$_{100-x}$Ag$_x$ modified electrodes towards the reduction of H_2O_2. All the four Au/Ag core–shell nanoparticles modified electrodes showed clear catalytic reduction of H_2O_2 from an onset potential of –0·15 V in the order of Au$_{73}$Ag$_{27}$ > Au$_{54}$Ag$_{46}$ > Au$_{40}$Ag$_{60}$ > Au$_{85}$Ag$_{15}$. This trend clearly indicates the synergistic catalytic effect of Au$_{73}$Ag$_{27}$ core–shell nanoparticles due to the optimum level of Ag shell thickness on Au core. This
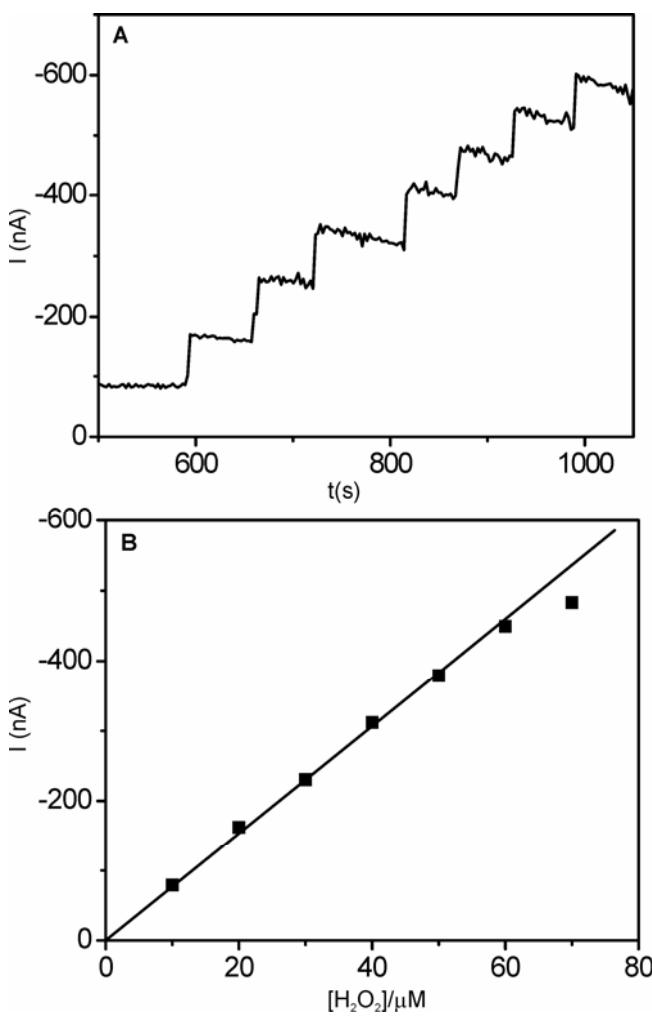

Figure 8. Current-time amperometric response observed for H_2O_2 at GC/MTMOS-Au$_{73}$Ag$_{27}$ electrode (**A**) during each addition of 10 μM H_2O_2 at an applied potential of –0·65 V (SCE) in 0·1 M PBS (pH = 7·2). Corresponding calibration plot observed for H_2O_2 at GC/MTMOS-Au$_{73}$Ag$_{27}$ electrode (**B**).
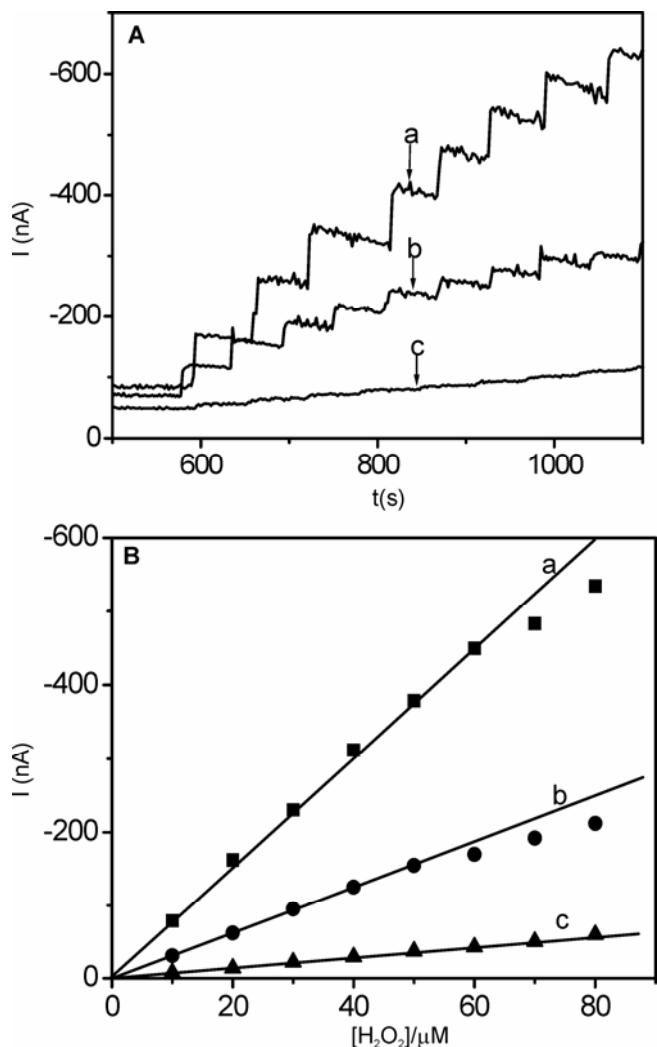
Figure 9. Current-time amperometric response observed for H_2O_2 at GC/MTMOSAu$_{73}$Ag$_{27}$ (a), GC/MTMOS-Au$_{nps}$ (b) and GC/MTMOS-Ag$_{nps}$ (c) electrodes (**A**) during each addition of 10 μM H_2O_2 at an applied potential of $-0\cdot65$ V(SCE) in $0\cdot1$ M PBS (pH = $7\cdot2$). Corresponding calibration plot (**B**) observed for H_2O_2 at GC/MTMOS-Au$_{73}$Ag$_{27}$ (a), GC/MTMOS-Au$_{nps}$ (b) and GC/MTMOS-Ag$_{nps}$ (c) electrodes.

observation reflects the EIS behaviour of Au$_{73}$Ag$_{27}$ composition at the MTMOS sol–gel matrix modified electrode.

3.7 *Chronoamperometric studies*

The GC/MTMOS-Ag$_{nps}$, GC/MTMOS-Au$_{nps}$ and GC/MTMOS-Au$_{73}$Ag$_{27}$ modified electrodes were used to construct amperometric sensor for H_2O_2 at pH $7\cdot2$. The current-time amperometric responses were recorded for the amperometric sensing of H_2O_2 using these modified electrode at an applied poten-

tial of $-0\cdot65$ V with subsequent spiking of 10 μM H_2O_2. The typical H_2O_2 amperometric and calibration curves based on the steady state H_2O_2 reduction current are shown in figures 8 and 9. Same amount of Au, Ag or Au/Ag (Ag$_{nps}$ or Au$_{nps}$ or Au$_{73}$Ag$_{27}$) was dispersed in the MTMOS sol–gel matrix. Figure 8A displays the amperometric curve and the H_2O_2 calibration curve based on the steady state H_2O_2 reduction current observed at the GC/MTMOS-Au$_{73}$Ag$_{27}$ modified electrode. Figure 8B shows the linear calibration line in the concentration range from 10 μM to 70 μM H_2O_2 with a correlation coefficient of $n = 0\cdot99$ at a signal to noise ratio of 3. The detection limit was experimentally estimated as 1 μM. The response time was found to be 3 s, which indicates a fast electron transfer process at the modified electrode. Figure 9A shows the comparison of current-time amperometric responses observed for H_2O_2 at GC/MTMOS-Ag$_{nps}$, GC/MTMOS-Au$_{nps}$ and GC/MTMOS-Au$_{73}$Ag$_{27}$ modified electrodes. The corresponding calibration plots are shown in figure 9B. It is clear that the Au/Ag core–shell bimetal nanoparticles embedded in MTMOS matrix acts as the best amperometric sensing device (figure 8B(a)) when compared to monometal Aunps and Ag$_{nps}$ in MTMOS matrix (figure 8B(b, c)). The detailed investigation to evaluate the electro-catalytic and sensing performance of the Au/Ag core–shell bimetal nanoparticles is in progress.

4. Summary

In summary, the cyclic voltammetry and chronoamperometric techniques were used to evaluate the electrocatalytic activities of Ag$_{nps}$, Au$_{nps}$ and Au/Ag core–shell nanoparticles embedded in MTMOS sol–gel matrix modified electrodes towards hydrogen peroxide reduction. It was observed that the molar composition of Ag shell on Au core in the Au/Ag bimetallic composition played a role in the electrocatalysis. The Au$_{73}$Ag$_{27}$ core–shell nanoparticles in MTMOS sol–gel matrix modified electrodes showed better electrocatalytic reduction of H_2O_2 when compared to monometal Au$_{nps}$ and Ag$_{nps}$ modified electrodes. The electrocatalysis was carried out with a large decrease in the over potential and in the absence of immobilized enzyme in the MTMOS sol–gel matrix when compared to that of monometals. Among the four different molar compositions of Au/Ag core–shell bimetallic nanoparticles, the Au$_{73}$Ag$_{27}$ nanoparticles showed better synergistic

catalytic effect towards the electrocatalytic reduction of H_2O_2. An amperometric sensor was constructed using this Au/Ag core–shell bimetallic nanoparticles embedded in MTMOS sol–gel matrix for sensing H_2O_2. The present work establishes the application of core–shell bimetal nanoparticles embedded in silicate sol–gel matrix towards electrocatalysis.

Acknowledgements

References

1. Michael S, Nashner A, Frenkel I, David L A, John, R S and Ralph G N 1997 *J. Am. Chem. Soc.* **119** 7760
2. Lehui L, Haishui W, Yonghui Z, Shiquan X, Hongjie Z, Jiawen H and Bing Z 2002 *Chem. Commun.* **2** 144
3. Alain R, Jurgen S and Henri P 2002 *Chem . Rev.* **102** 3757
4. Park J Y, Zhang Y, Grass M, Zhang T and Somorjai G A 2008 *Nano Lett.* **8** 673
5. Toshima N and Wang Y 1994 *Langmuir* **10** 4574
6. Yang Y, Khalil A A and Lisa M W 2003 *Dalton Trans.* **22** 4288
7. Daniel M C and Astruc D 2004 *Chem. Rev.* **104** 293
8. Tasis D, Tagmatarchis N, Bianco A and Prato M 2006 *Chem. Rev.* **106** 1105
9. Thomas K G and Kamat P V 2003 *Acc. Chem. Res.* **36** 888
10. Mayya K S, Schoeler B and Caruso F 2003 *Adv. Funct. Mater.* **13** 183
11. Shirlaine K and Peter S 2007 *J. Am. Chem. Soc.* **129** 12624
12. Rivas L, Cortes S S, Ramos V G and Morcillo G 2000 *Langmuir* **16** 9722
13. Joseph W 2005 *Analyst* **4** 421
14. Lev O, Tsionsky M, Rabinovich L, Glezer V, Sampath S, Pankratov I and Gun J 1995 *Anal. Chem.* **67** 22A
15. Dave B C, Dunn B, Valentine J S and Zink J I 1994 *Anal. Chem.* **66** 1120A
16. Soo B K and Fang C 2002 *Anal. Chem.* **74** 5734
17. Lin J and Brown C W 1997 *Anal. Chem.* **16** 200
18. Cushing B L, Kolesnichenko V L and O'Connor C J 2004 *Chem. Rev.* **104** 3893
19. Holstrom S D and Cox J A 2000 *Anal. Chem.* **72** 3191
20. Rubianes M D and Rivas G A 2003 *Electrochem. Commun.* **5** 689
21. Rubianes M D and Rivas G A 2005 *Electroanalysis* **17** 73
22. Tetsu T and Tadashi W 1991 *Anal. Chem.* **63** 1580
23. Gao F, Yuan R, Chai Y, Tang M, Cao S and Chen S 2007 *Colloids and surfaces: A physicochemical and engineering aspects* **295** 223
24. Wu S, Zhao H, Ju H, Shi C and Zhao J 2006 *Electrochem. Commun.* **8** 1197
25. Yang W, Li Y, Bai Y and Sun C 2006 *Sensors and Actuators* **B115** 42
26. Hill H A 1996 *Coord. Chem. Rev.* **151** 233
27. Wang J, Musameh M and Lin Y 2003 *J. Am. Chem. Soc.* **125** 2408
28. Li X, Heryadi D and Gewirth A A 2005 *Langmuir* **21** 9251
29. Cooper J M, Greenough K R and Mencil C J 1993 *J. Electroanal. Chem.* **347** 267
30. Kim J and Gewirth A A 2005 *J. Phys. Chem.* **B109** 9684
31. Frenz G 1973 *Nature* **241** 20
32. Lee P C and Meisel D 1982 *J. Phys. Chem.* **86** 3391
33. Sbkhoo K 2002 *Anal. Chem.* **74** 5734
34. Maduraiveeran G and Ramaraj R 2007 *J. Electroanal. Chem.* **52** 58
35. Mie G 1908 *Ann. Phys.* **25** 377
36. Benito R G, Ana S I, Micheal G, Luis M and Liz M 2004 *Faraday Discuss.* **125** 133
37. Zhang L, Jiang X, Wang E and Dong S 2005 *Biosens. Bioelectron.* **21** 337
38. Feng J, Zhao G, Xu J and Chen H 2005 *Anal. Biochem.* **342** 280
39. Zeng J, Yang J, Lee J Y and Zhou W 2006 *J. Phys. Chem.* **B110** 24606